Available online at www.sciencedirect.com
ScienceDirect
Journal of Molecular Catalysis A: Chemical 273 (2007) 177–185
JOURNAL OF MOLECULAR CATALYSIS A: CHEMICAL
www.elsevier.com/locate/molcata

Sol–gel preparation and characterization of alkaline earth metal doped nano TiO_2: Efficient photocatalytic degradation of 4-chlorophenol

N. Venkatachalam, M. Palanichamy, V. Murugesan *

Department of Chemistry, Anna University, Chennai 25, India

Received 12 February 2007; received in revised form 28 March 2007; accepted 31 March 2007
Available online 7 April 2007

Abstract

Magnesium and barium doped TiO_2 nanoparticles were synthesized by sol–gel method. The materials were characterized by XRD, BET, FT-IR, TGA, UV–vis, SEM and TEM techniques. The pure TiO_2 nanoparticles contained both anatase and rutile phases together, but Mg^{2+} or Ba^{2+} metal ion doped nano TiO_2 gave only anatase phase. The framework substitution of Mg^{2+} in nano TiO_2 was established by XRD and FT-IR techniques. However, Ba^{2+} was retained only on the surface of nano TiO_2 as $BaCO_3$ and the absence of framework substitution of Ba^{2+} in nano TiO_2 was evident from XRD and FT-IR analysis. The band gap values of Mg^{2+} and Ba^{2+} doped nano TiO_2 were higher than the pure nano TiO_2. The presence of anatase type structure in nano TiO_2 with high crystallinity and high phase stability even after annealing at 800 °C substantially indicates that the dopants might inhibit densification and crystallite growth in nano TiO_2 by providing dissimilar boundaries. The photocatalytic activity in the degradation of 4-chlorophenol was found to be higher for Mg^{2+} and Ba^{2+} doped nano TiO_2 than both pure nano TiO_2 and commercial TiO_2 (Degussa P-25). The influence of various parameters such as initial concentration of 4-chlorophenol, catalyst loading, pH and light intensity were optimized to obtain maximum degradation.

Keywords: Nano TiO_2; Metal doping; Anatase phase; Endocrine disruptor; Mineralization

1. Introduction

Effluents discharged from industries contain toxic organic chemicals, which need to be treated prior to disposal. 4-Chlorophenol (4-CP), a known endocrine disruptor is toxic and non-biodegradable, present in wastewater as by-products of pulp and paper, dyestuff, pharmaceutical and agrochemical industries [1,2]. Conventional wastewater treatment methods like chemical precipitation, activated carbon adsorption and ion-exchange processes are usually effective in the removal of these compounds in wastewater. However, they transfer the contaminants from one medium to another and hence further treatment or disposal is required. Biodegradation of 4-CP is not only slow and incomplete but also the by-products are more toxic than the contaminants [3–5]. Photocatalysis has been reported as an effective method for treating a wide range of pollutants both from water and air. TiO_2 has emerged as the most viable semiconductor photocatalyst as it is stable in aqueous medium and is tolerant to both acidic and alkaline media [6,7].

There are a few drawbacks associated with the use of bulk TiO_2 like charge carrier recombination occurring within nanoseconds, and the band edge absorption threshold preventing utilisation of visible light. To circumvent these limitations, a number of strategies have been attempted to improve the photocatalytic activity of TiO_2. The photocatalytic efficiency of TiO_2 can be enhanced by three methods, namely, increasing its surface to volume ratio, sensitization using dye molecules and doping of metals and non-metals [8–11]. The high surface to volume ratio inherent in nanoparticles is useful for photocatalysis and hence most of the studies are focused on the nanosized TiO_2 with the purpose of improving the light absorption. The dye sensitized TiO_2 has been used for improving the TiO_2 efficiency particularly in photovoltaics. Unfortunately, the known sensitizers are toxic or unstable in aqueous medium, thus making them inappropriate for application in photocatalysis. The enhancement of photoactivity of TiO_2 has been demonstrated using dopant metal ions or oxides to modify the band gap or to act as charge separators of the photoinduced electron–hole pair [12,13].

* Corresponding author. Tel.: +91 44 22203144; fax: +91 44 22200660/22350397.
E-mail address: v_murugu@hotmail.com (V. Murugesan).

1381-1169/$ – see front matter © 2007 Elsevier B.V. All rights reserved.
doi:10.1016/j.molcata.2007.03.077

Transition metal ion dopants were investigated previously for TiO_2 using wet-impregnation method in order to minimize e^-/h^+ recombination process, among which Fe^{3+} has been most widely examined [14]. Most of the metal doped TiO_2 reported in the literature were prepared by co-precipitation or incipient wet impregnation method [15,16]. Substitution of metal ions in the bulk TiO_2 crystallites is not likely to occur and at the best substitution may take place on the surface of TiO_2 in the impregnation method. In the co-precipitation method, post heat processing of mixed metal hydroxides yields metal doped TiO_2. This high temperature and long time heating may separate out the dopant metal ions into respective metal oxides, and in many cases they segregate on the surface [17]. In order to overcome such problems, sol–gel technique has been adopted as one of the versatile methods for the preparation of metal doped nanocrystalline TiO_2. Since this method is a solution process, it allows flexibility in parameter control with its relatively slow reaction process. This permits tailoring of certain desired structural characteristics such as compositional homogeneity, grain size, particle morphology and porosity. Sol–gel preparation of transition metal doped nano TiO_2, characterization and its photocatalytic activity have been reported in the recent literature [18–21]. Sol–gel preparation of alkaline earth metal doped nano TiO_2 is not widely reported. The physico-chemical properties of alkaline earth metal doped nano TiO_2 and correlation of these properties in the degradation of 4-CP are presented in this manuscript.

2. Experimental

2.1. Materials and methods

All the chemicals were obtained from Merck (India) and used as such without further purification. The commercially available TiO_2 (Degussa P-25) was obtained from Degussa Chemical, Germany. The typical synthesis procedure for nano TiO_2 and metal doped nano TiO_2 is as follows: Titanium(IV) isopropoxide, glacial acetic acid and water were maintained in a molar ratio 1:10:350. Titanium(IV) isopropoxide (18.6 ml) was hydrolyzed using glacial acetic acid (35.8 ml) at 0 °C. To this solution 395 ml water was added drop wise under vigorous stirring for 1 h and continued the stirring for further 1 h until a clear solution of TiO_2 nano crystals was formed. The prepared solution was kept in dark for nucleation process for 12 h. After the period, the solution was placed in an oven at a temperature of 70 °C for a period of 12 h for gelation process. The gel was then dried at 100 °C and subsequently the catalyst was crushed into fine powder and calcined in a muffle furnace at 500 °C for 5 h. For the preparation of Ba^{2+} and Mg^{2+} doped nano TiO_2, requisite amount of barium or magnesium nitrate (0.3, 0.5, 0.7, 1.0, 2.0 and 3.0 mol%) was dissolved in 395 ml water and the above procedure was adopted as such.

2.2. Analytical methods for catalyst characterization

The XRD patterns were recorded on a PANAalytical X' pert PRO X-ray diffractometer using Cu Kα radiation as the X-ray source. The diffractograms were recorded in the 2θ range 10–80° in steps of 0.02° with a count time of 20 s at each point. The average crystallite size of anatase and rutile phases was determined according to the Scherrer equation using the full width at half maximum (FWHM) data of each phase after correcting the instrumental broadening. The specific surface area (BET method), specific pore volume and average pore diameter (BJH method) of the samples were determined by nitrogen adsorption–desorption isotherms using Quantochrome Autosorb 1 sorption analyzer. The calcined samples were outgassed at 250 °C under vacuum (10^{-5} mbar) for 3 h prior to adsorption experiments. The particle size and morphology of nano TiO_2, Ba^{2+} and Mg^{2+} doped nano TiO_2 were observed using scanning electron microscope (SEM) (Stereoscan LEO 440) and transmission electron microscope (TEM) (JEOL 3010). The emission spectra of the catalyst samples were recorded using spectrofluorometer (Horiba Fluromax-2) at an excitation wavelength of 290 nm. UV–vis absorption spectra of the samples were recorded using UV–vis spectrophotometer (Shimadzu 2601). FT-IR spectra of the samples were recorded on a FT-IR spectrometer (Nicolet Avatar 360). Thermograms of the samples were recorded using thermogravimetric analyzer (TG/DTA) (Perkin-Elmer Diamond). The extent of 4-CP degradation was monitored using UV–vis spectrophotometer (Shimadzu 1601) and high performance liquid chromatograph (HPLC) (Shimadzu LC10 ATVP series equipped with UV–vis detector). The intermediates were identified using gas chromatograph coupled with mass spectrometer (GC–MS) (Perkin-Elmer Clarus 500). The extent of mineralization was determined using a total organic carbon analyzer (TOC) (Shimadzu V_{CPN}).

2.3. Adsorption study

Prior to photocatalytic experiments, adsorption study of 4-CP on the catalyst surface was carried out by mixing 100 ml aqueous solution of 4-CP (250 mg/l) with a fixed weight of the catalyst (200 mg) at a pH 5. Aliquots were withdrawn at specific time intervals and the change in 4-CP concentration was measured by HPLC. The extent of equilibrium adsorption was determined from the decrease in 4-CP concentration. From the adsorption experiments, the percentage of 4-CP adsorbed on the catalyst surface was determined from the following equation:

$$\%\text{of 4-CP adsorbed} = \frac{C_0 - C_t}{C_0} \times 100$$

where C_0 is the initial concentration of 4-CP and C_t is the concentration of 4-CP after 't' minutes.

2.4. Photocatalytic studies

The photocatalytic degradation of 4-CP was carried out in a slurry photocatalytic reactor. The design description of photocatalytic reactor was reported in our earlier study [22]. The experimental conditions were: initial concentration of 4-CP = 250 mg/l, volume of 4-CP = 100 ml, solution pH 5 and catalyst dosage = 200 mg. The experiments were performed at room temperature. Prior to UV irradiation, the slurry was aerated for 30 min to reach adsorption equilibrium. Adequate aliquot

of the sample was withdrawn after periodic interval of irradiation and analysed after centrifugation for degradation and mineralization.

3. Results and discussion

3.1. Physico-chemical characterization

The XRD patterns of nano TiO_2 and magnesium doped nano TiO_2 are shown in Fig. 1. The patterns of calcined (500 °C) nano TiO_2 correspond to both anatase and rutile phases (Fig. 1a) with the former is the predominant one. The XRD patterns of 1 mol% Mg^{2+} doped nano TiO_2 indicate the absence of rutile phase (Fig. 1b). It can be seen that increase of calcination temperature from 400 to 700 °C, the peak intensity of anatase increases and the width of (1 0 1) plane at $2\theta = 25.3°$ becomes narrow. The rutile phase starts appearing at 500 °C for pure nano TiO_2 whereas the rutile peaks appear only at 700 °C for Mg^{2+} doped nano TiO_2. Thus, the dopant is expected to play a significant control in the selective crystallisation of anatase phase during sol–gel process [23]. The close examination of XRD patterns of both nano TiO_2 and Mg^{2+} doped nano TiO_2 illustrates the existence of splitting of peaks at 37.74°, 48.19°, 55°, 62.79°, 68.77° and 75.09° (2θ). Further, the intensity of anatase peaks decreases due to Mg^{2+} doping. These observations establish the presence of Mg^{2+} in the lattice of nano TiO_2. This is further confirmed by FT-IR analysis.

As there is no evidence in the XRD patterns for isomorphic substitution of Ba^{2+} in nano TiO_2, it is expected that Ba^{2+} is present on the surface of nano TiO_2. This is quite reasonable as the ionic radius of Ba^{2+} is larger than Ti^{4+}. Furthermore, the XRD patterns of uncalcined 1 mol% Ba^{2+} doped nano TiO_2 showed (Fig. 2a) less intense peaks, and all these peaks correspond to anatase phase only. Again there is no evidence for the formation of crystalline barium oxide phase. The XRD patterns of calcined 1 mol% Ba^{2+} doped nano TiO_2 (Fig. 2b) showed the existence of anatase phase. The peaks at 23.90°, 34.0°, 42.19° and 46.78° (2θ) correspond to $BaCO_3$ [24]. Hence, there might

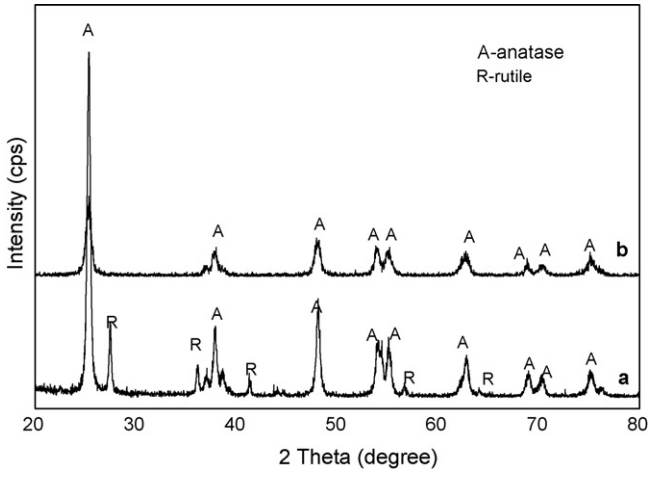

Fig. 1. XRD patterns of (a) nano-TiO_2 and (b) 1 mol% Mg^{2+} doped nano TiO_2 calcined at 500 °C.

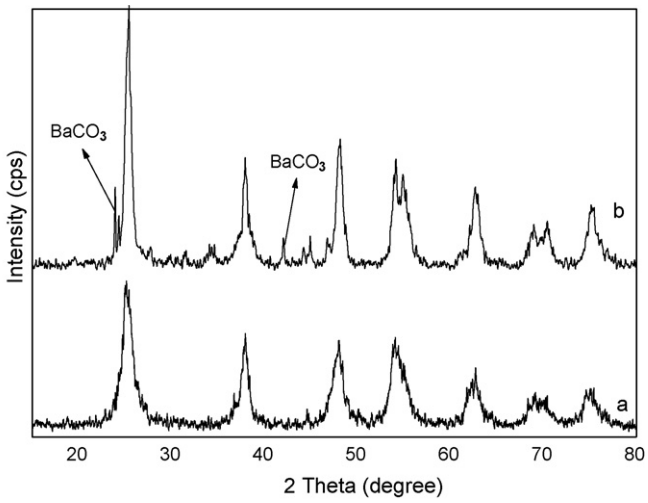

Fig. 2. XRD patterns of 1 mol% Ba^{2+} doped nano TiO_2 (a) uncalcined and (b) calcined at 500 °C.

be formation of BaO, which is subsequently converted to $BaCO_3$ during calcination of 1 mol% Ba^{2+} doped nano TiO_2. As a result of calcination, there is enhanced intensity for all the patterns compared to uncalcined nano TiO_2. Hence, there might be condensation of free defective OH groups to form nano TiO_2 with high percentage of crystallinity. Since Ba^{2+} is more electropositive, the electronic cloud in each TiO_2 nano particle might be loosely held, thus favouring the formation of less dense anatase phase. In other words, the tight packing arrangement required for rutile phase formation is fully suppressed by the addition of barium nitrate in water which enhances the polarity of water, thus facilitating the formation of anatase phase exclusively. Further, the peaks corresponding to $MgCO_3$ or MgO do not exist in the case of 1 mol% Mg^{2+} doped nano TiO_2 but the intensity of anatase peaks decreases. This is due to the formation of nano-sized TiO_2 particles in the range undetectable by XRD. TEM analysis has shown the formation of TiO_2 particles of size less than even 4 nm.

During the sol–gel synthesis of metal doped nano TiO_2, high water content was kept to enhance the nucleophilic attack of water on titanium(IV) isopropoxide and to suppress fast condensation of titanium(IV) isopropoxide species to yield TiO_2 nanocrystals. In addition, the presence of residual alkoxy groups can significantly reduce the rate of crystallization of nano TiO_2 which favoured the formation of less dense anatase phase [25]. Further, among the two main kinds of crystalline TiO_2, anatase is proved to exhibit higher photocatalytic activity in the degradation of most pollutants in water and air, while the photocatalytic activity of rutile is still indistinct. Many reports have revealed that the rutile form of TiO_2 is a poor photocatalyst [26,27]. The reasons for this could be attributed that the adsorptive affinity of anatase for organic compounds is higher than that of rutile, and the anatase phase also exhibits low rate of recombination in comparison to rutile due to its ten fold greater rate of hole trapping [28]. Furthermore, the preparation of nano TiO_2 and Ba^{2+} and Mg^{2+} doped nano TiO_2 were carried out in presence of acetic acid. Since pK_a of acetic acid is close to three, there is every chance for protonation of TiO_2 nano particles which could

Table 1
Textural and structural properties of nano and metal doped nano TiO_2

Catalyst	Specific surface area (m^2/g)[a]	Pore volume (cm^3/g)[b]	Pore diameter (nm)[c]	Particle size (nm)[d]	Bandgap energy (eV)[e]	4-CP adsorbed (%)
Nano TiO_2	66	0.209	3.6	18–20	3.21	13.2
0.5 mol% Mg^{2+}–TiO_2	89	0.247	4.2	12–15	3.27	24.8
1.0 mol% Mg^{2+}–TiO_2	112	0.323	4.8	6–10	3.29	35.4
1.0 mol% Ba^{2+}–TiO_2	96	0.314	4.6	8–12	3.26	37.2
3.0 mol% Mg^{2+}–TiO_2	81	0.211	3.8	4–12	3.31	41.5
3.0 mol% Ba^{2+}–TiO_2	76	0.194	3.6	10–12	3.26	44.2

[a] BET surface area calculated from the linear portion of the BET plot in the relative pressure range of $p/p_0 = 0.05$–0.35.
[b] Total pore volume taken from the volume of N_2 adsorbed at about $p/p_0 = 0.995$.
[c] Average pore diameter estimated using adsorption branch of the isotherm.
[d] Particle size obtained from TEM pictures.
[e] Band gap energy calculated using the formula (E_{bg}) = 1240/λ.

suppress further crystallization. In addition, the excess acetate anion adsorbed on the surface of TiO_2 could also suppress the growth of nano TiO_2. This type of complexation of acetate anion on the surface of anatase form of TiO_2 may be responsible for the decrease in the crystallite size of TiO_2 in the sol–gel synthesis. The addition of acetic acid did not cause residual impurities on the surface of TiO_2 after calcination, which was confirmed from the FT-IR spectral study.

The data of textural properties of nano TiO_2, Mg^{2+} and Ba^{2+} doped nano TiO_2 are presented in Table 1. The specific surface area is higher for 1 mol% Mg^{2+} and Ba^{2+} doped nano TiO_2 than pure nano TiO_2 and TiO_2 (Degussa P-25). Fig. 3. illustrates the pore size distribution calculated from the desorption branch of nitrogen isotherm by BJH method and the corresponding nitrogen adsorption–desorption isotherm of 1 mol% Mg^{2+} doped nano TiO_2 calcined at 500 °C for 5 h. The occurrence of hysteresis loop (type IV) demonstrated the existence of mesoporosity in doped nano TiO_2. These pores may allow rapid diffusion of 4-CP molecules during photocatalytic reactions, and also enhance the adsorption of 4-CP and its intermediates on nano TiO_2 surface.

FI-IR spectra of pure and metal doped nano TiO_2 showed peaks corresponding to stretching vibrations of O–H and bending vibrations of adsorbed water molecules around 3350–3450 and 1620–1635 cm^{-1}, respectively. The intensity of these peaks became less with increase of calcination temperature, indicating the removal of large portion of adsorbed water from TiO_2 (not shown in figure). The broad intense band below 1200 cm^{-1} is due to Ti–O–Ti vibration (Fig. 4a). This peak appears quite unsymmetrical whereas the same for 1 mol% Mg^{2+} doped nano TiO_2 appears symmetrical. There is significant shift in the peak maximum to high energies in the FT-IR spectrum of Mg^{2+} doped nano TiO_2 compared to parent nano TiO_2. Since the atomic mass of magnesium is lower than titanium, one could expect shifting of Ti–O–Mg vibration to higher energy than Ti–O–Ti vibration. In addition, the new peak appeared at 1015 cm^{-1} (Fig. 4b) is also taken into consideration for isomorphic substitution. This peak is tentatively assigned to framework Ti–O–Mg vibration. This additional peak was not observed in Ba^{2+} doped nano TiO_2. Hence FT-IR spectral study established clearly the entry of Mg^{2+} and not Ba^{2+} into the lattice of nano TiO_2. The FT-IR spectra of uncalcined and calcined 1 mol% Ba^{2+} doped nano TiO_2 are shown in Fig. 5. There is a peak at 1400 cm^{-1} in the spectrum of

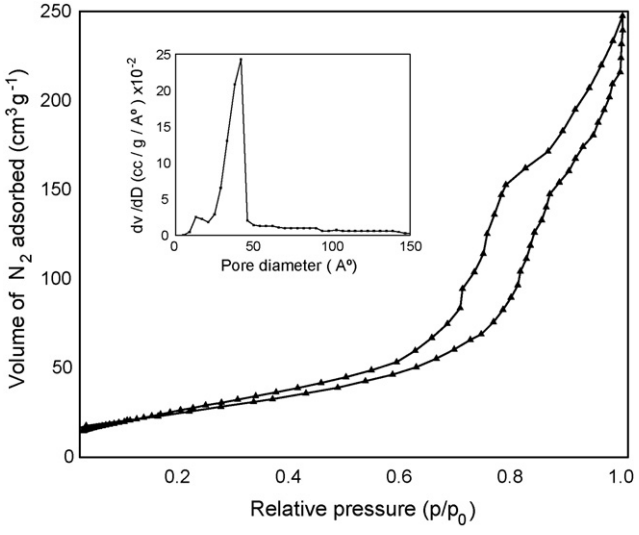

Fig. 3. Nitrogen adsorption–desorption isotherms and the corresponding pore size distribution curve calculated from desorption branch of the nitrogen isotherm (inset) of 1 mol% Mg^{2+} doped nano TiO_2 calcined at 500 °C.

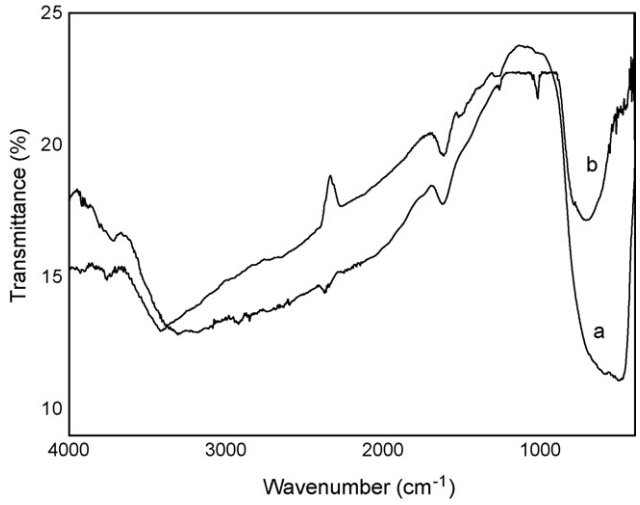

Fig. 4. FT-IR spectra of (a) nano-TiO_2 and (b) 1 mol% Mg^{2+} doped nano TiO_2 calcined at 500 °C.

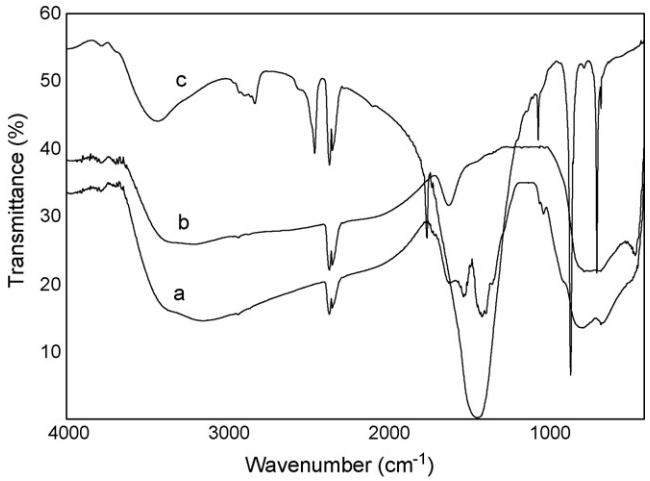

Fig. 5. FT-IR spectra of (a) 1 mol% Ba^{2+} doped nano TiO_2 (calcined at 500 °C), (b) 1 mol% Ba^{2+} doped nano TiO_2 (uncalcined) and (c) $BaCO_3$.

calcined 1 mol% Ba^{2+} doped nano TiO_2 but this peak is absent in the spectrum of uncalcined 1 mol% Ba^{2+} doped nano TiO_2. BaO formed during calcination of 1 mol% Ba^{2+} doped nano TiO_2 subsequently absorbed CO_2 to form $BaCO_3$. The spectrum of $BaCO_3$ is also shown (Fig. 5c) in order to confirm the formation of $BaCO_3$ in nano TiO_2. There is an intense broad peak close to 1400 cm^{-1} in the spectrum of $BaCO_3$ which is due to carbonate vibration. FT-IR studies clearly indicate the presence of $BaCO_3$ layer in Ba^{2+} doped nano TiO_2.

SEM and TEM pictures confirmed that the metal doped nano TiO_2 particles are spherical in shape with an average grain size of 8–10 nm. Further, the SEM picture (Fig. 6) of 1 mol% Ba^{2+} doped nano TiO_2 showed deposits of irregular shape particles over nano TiO_2 surface, and these tiny particles may be assigned as insoluble $BaCO_3$. Fig. 7 illustrates the TEM picture of 1 mol% Ba^{2+} doped nano TiO_2. Fig. 8 shows the histogram (particle size distribution) of 1 mol% Mg^{2+} doped nano TiO_2. Both pictures clearly showed the nanocrystalline nature of TiO_2 obtained from the hydrolysis of titanium(IV) isopropoxide. Furthermore, the TEM picture (Fig. 7) of 1 mol% Ba^{2+} doped nano TiO_2 also

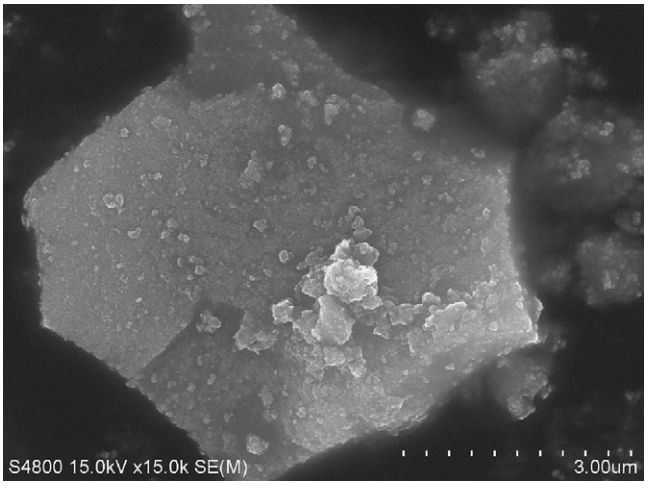

Fig. 6. SEM picture of 1 mol% Ba^{2+} doped nano TiO_2 calcined at 500 °C.

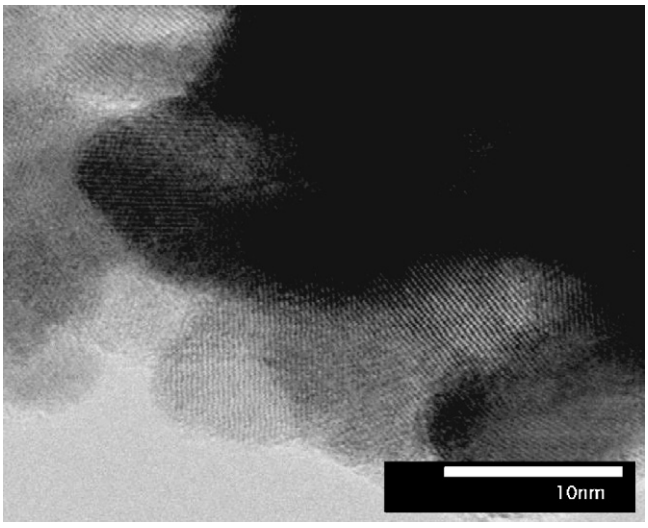

Fig. 7. TEM picture of 1 mol% Ba^{2+} doped nano TiO_2 calcined at 500 °C.

gave convincing evidence for the presence of barium carbonate layer on the surface nano TiO_2.

The thermograms of nano TiO_2, 1 mol% Mg^{2+} and Ba^{2+}doped nano TiO_2 are shown in Fig. 9. The weight loss occurred up to 400 °C and these weight losses occurred in three stages for Ba^{2+} doped nano TiO_2. This observation revealed that Ba^{2+} might be in the form of BaO, $Ba(OH)_2$ and/or $BaCO_3$. Since the decomposition temperature of $BaCO_3$ is 1450 °C, the weight loss below 400 °C might be due to the removal of adsorbed water on TiO_2, decomposition of $Ba(OH)_2$ (water and BaO) and desorption of water from BaO. UV–vis absorption spectra of pure, Mg^{2+} and Ba^{2+} doped nano TiO_2 are depicted in Fig. 10. The absorption spectrum of pure nano TiO_2 consists of a single and broad intense absorption around 400 nm due to charge-transfer from the valence band (mainly formed by 2p orbitals of the oxide anions) to the conduction band (mainly formed by 3d t_{2g} orbitals of the Ti^{4+} cations) [29]. Pure nano TiO_2 showed absorption in the longer wavelength region than the metal doped nano TiO_2. Hence, there might be sufficient

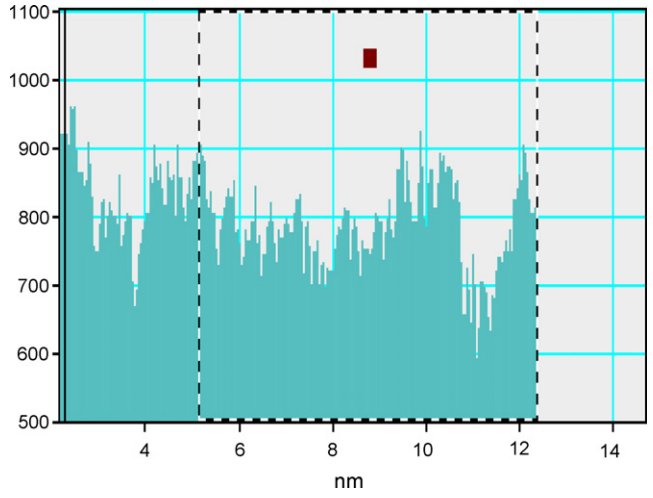

Fig. 8. Particle size distribution histogram of 1 mol% Mg^{2+} doped nano TiO_2 calcined at 500 °C.

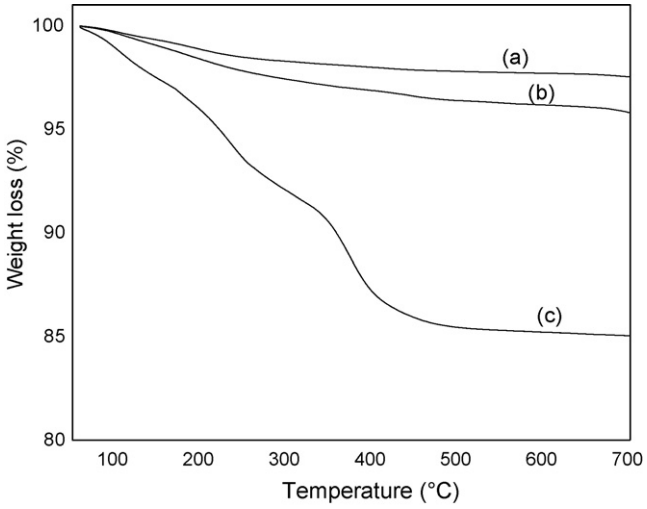

Fig. 9. Thermograms of (a) TiO_2 (Degussa P-25), (b) 1 mol% Mg^{2+} doped nano TiO_2 and (c) 1 mol% Ba^{2+} doped nano TiO_2.

decrease in the particle size and increase in the band gap value due to Mg^{2+} doping. The formation of large number of nano particles in doped nano TiO_2 in comparison to pure TiO_2 is also evident from the difference in the height of absorbance of pure nano TiO_2, Mg^{2+} and Ba^{2+} doped nano TiO_2.

This study clearly established the role of Mg^{2+} and Ba^{2+} in decreasing the size of nano TiO_2. Ba^{2+} inhibits the densification and crystallite growth of nano TiO_2 during calcination process by providing dissimilar boundaries. The fluorescence emission spectra of nano and Ba^{2+} and Mg^{2+} doped nano TiO_2 are presented in Fig. 11. The emission spectra of Mg^{2+} doped nano TiO_2 give convincing evidence for the oxygen vacancy in nano TiO_2. Since the excitation was carried out under equal adsorption conditions at 290 nm, decrease in emission intensity was observed with Mg^{2+} doped nano TiO_2 samples compared to pure nano TiO_2. The decrease in the emission intensity may also due to introduction of new defect sites such as oxide ion vacancy [17]. The oxide ion vacancy can trap an electron in the following pathway. The ionized oxygen vacancy level is poised to trap rapidly the photogenerated conduction band electron which subsequently interacts with a valence band hole either radiatively or non-radiatively.

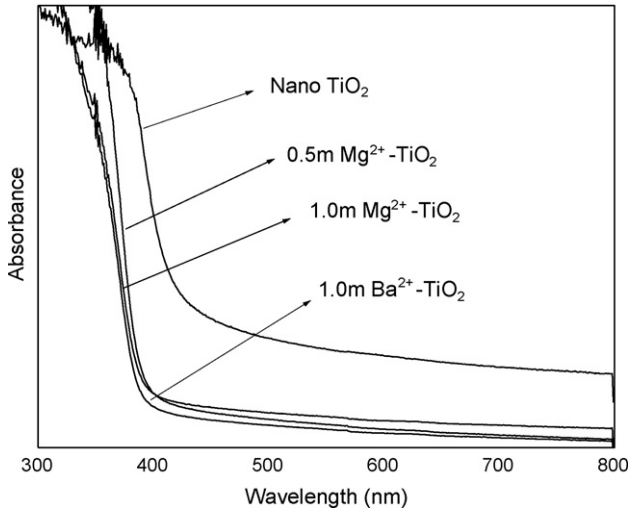

Fig. 10. UV–vis absorption spectra of nano TiO_2 and Mg^{2+} and Ba^{2+} doped nano TiO_2 calcined at 500 °C.

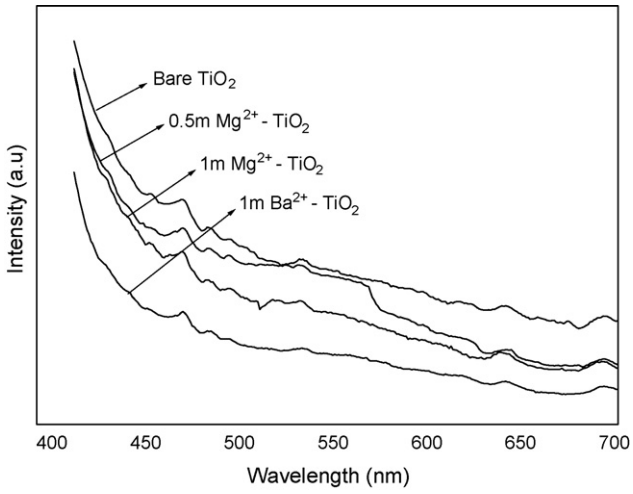

Fig. 11. Emission spectra of nano TiO_2 and Mg^{2+} and Ba^{2+} doped nano TiO_2 calcined at 500 °C.

$$V_o^0 + e_{CB}^- \rightarrow V_0 \quad \text{(electron trapping in shallow traps)}$$

$$V_0 + h_{VB}^+ \rightarrow V_o^0 + h\nu \quad \text{(radiative recombination)}$$

Ba^{2+} doped nano TiO_2 also exhibited less intensity of emission than pure nano TiO_2. This low intensity emission is ascribed to low absorption of light by Ba^{2+} doped nano TiO_2 due to the formation of $BaCO_3$ layer on its surface. In other words, the carbonate layer may block significantly the entry of UV light into TiO_2 particles to excite electrons.

3.2. Photocatalytic degradation of 4-CP

Chlorophenols are listed as endocrine disruptors by EPA and considered as priority pollutants. Photocatalytic oxidation is a promising alternative to the conventional methods for the complete mineralization of 4-CP. The efficiency of photocatalytic degradation process depends on various experimental parameters such as initial concentration of the pollutant, catalyst loading, pH, light intensity and irradiation time. Hence it is essential to optimize these parameters to achieve higher degradation efficiency for photocalytic degradation of 4-CP.

3.2.1. Effect of initial 4-CP concentration

The influence of initial 4-CP concentration on degradation rate was studied from 50 to 300 mg/l at a constant nano TiO_2 loading of 200 mg and a solution pH of 5. The volume of 4-CP solution was 100 ml. It is observed that the degradation rate increases with increase in concentration of 4-CP up to 250 mg/l and then decreases. The degradation follows pseudo-first-order kinetics at low 4-CP concentration, which is in accordance with our earlier reports [30]. The UV λ_{max} value of 4-CP is 280 nm. Hence, the absorption of UV light by the 4-CP will predominate at higher concentrations. The screening effect dominates

at concentrations higher than 250 mg/l and hence degradation efficiency decreases. We have observed such type of screening effect in the degradation of dyes and pesticides in our earlier reports [30]. Furthermore, the formation of (OH radicals is constant for a given quantity of the catalyst and hence the available (OH radicals are insufficient for 4-CP degradation at higher concentration.

3.2.2. Effect of catalyst dosage

A series of experiments were carried out to obtain the optimum catalyst loading by varying the amount of nano TiO_2 from 100 to 500 mg in 100 ml 4-CP solution of concentration 250 mg/l. The rate of degradation increases linearly with increase in catalyst loading up to 200 mg and then decreases due to increase in turbidity of the solution, which interfere the penetration of light transmission. The low degradation rate at higher catalyst loading may also due to deactivation of activated molecules by collision with ground state molecules of titania [31].

3.2.3. Effect of solution pH

Solution pH is an important variable in the evaluation of aqueous phase mediated photocatalytic degradation reactions. It influences adsorption and dissociation of the substrate, catalyst surface charge, oxidation potential of the valence band and other physico-chemical properties. The role of pH on the rate of photocatalytic degradation was attempted under optimum concentration of 4-CP (250 mg/l) and nano TiO_2 (200 mg) by varying the initial pH values from 4 to 9. It is reported that the zero point charge (pH_{zpc}) of TiO_2 is 6.9. The rate of degradation in the acidic pH range (at 5) was found to be higher than the alkaline pH. The high degradation rate in the acidic pH range is due to enhanced adsorption of 4-CP on the surface of nano TiO_2 that carries positive charge. In addition, minimization of electron–hole recombination in the acidic pH is also an additional important factor for the enhancement of degradation. In the alkaline pH (at 9) both 4-CP and surface of nano TiO_2 carry negative charge and hence the degradation rate was found to be less.

3.2.4. Effect of light intensity

The effect of light intensity was investigated in the range of 16–64 W. The results reveal that the degradation rate increases with increase in the light intensity up to 64 W. The excitation of every catalyst particle by light irradiation at any instant is not possible but increasing the intensity of incident light, the probability of excitation can be increased. It also increases the reexcitation of recombined electrons. Hence increase in the degradation rate is observed with increase in the intensity of incident light. The mineralization of 4-CP was studied over nano TiO_2 with lamp of wavelength 365 nm and compared with that of 254 nm. Though mineralization rates apparently appear to be nearly equal for both the lamps, the mineralization rate at 365 nm is slightly higher than at 254 nm. Since the band gap excitation of electrons in TiO_2 with 254 nm can promote electrons to the conduction band with high kinetic energy, they can reach the solid-liquid interface easily, suppressing electron–hole recombination in comparison to 365 nm. Hence the observation of low rate at 254 nm is therefore unexpected. This can be accounted by considering partial absorption and wasting of light of 254 nm by 4-CP itself. Generally, the pollutant must have negligible absorption close to the wavelength of irradiation source. Hence the entire light of irradiation at 254 nm in the reactor is not used for the excitation of TiO_2 particles because of the intervening 4-CP molecules as well as those adsorbed on TiO_2 particles. Hence absorption and wasting of light at 254 nm by 4-CP might be the actual cause for less rate of degradation than at 365 nm.

3.2.5. Mineralization studies

The extent of degradation and mineralization of 4-CP was followed by UV–vis spectroscopy, HPLC and TOC analyzer. Compounds like hydroquinone and hydroxyhydroquinone were the predominant intermediates formed during the photocatalytic degradation of 4-CP, which were identified by GC–MS. Hydroquinone retained for longer period during the photocatalytic degradation of 4-CP. This may be due to the fact that hydroquinone in acidic medium can exist in equilibrium with quinone as shown in the following Eq. (1). The released electrons thus neutralize the holes of nano TiO_2. The electron in the conduction band can also easily trapped by quinone to form hydroquinone. Hence, the mineralization of hydroquinone by photocatalytic degradation is rather difficult.

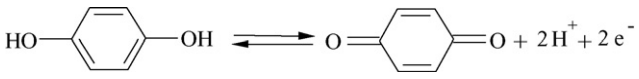

(1)

The decreasing trend of TOC against irradiation time in the degradation of 4-CP using Ba^{2+} and Mg^{2+} doped nano TiO_2, nano TiO_2 and TiO_2 (Degussa P-25) are depicted in Fig. 12. The TOC removal efficiency of TiO_2 (Degussa P-25) and nano TiO_2 is lower than that of Mg^{2+} and Ba^{2+} doped nano TiO_2. Under identical and optimal experimental conditions, 1 mol%

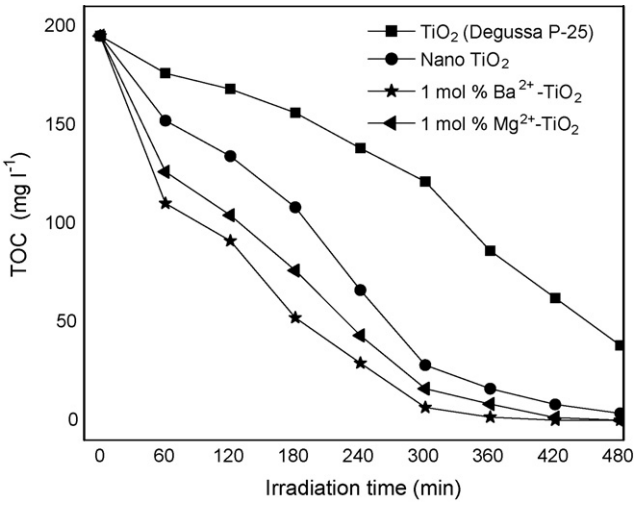

Fig. 12. Comparison of photocatalytic mineralization of TiO_2 (Degussa P-25), nano TiO_2 and metal doped nano TiO_2 (experimental conditions: initial concentration of 4-CP = 250 mg/l, volume of 4-CP = 100 ml, solution pH 5 and catalyst dosage = 200 mg).

Mg^{2+} and Ba^{2+} doped nano TiO_2, nano TiO_2 and TiO_2 (Degussa P-25) required 300, 360 and 450 min respectively for complete mineralization of 4-CP.

3.2.6. Role of alkaline earth metals in nano TiO_2

The analytical results revealed that dopants in nano TiO_2 play a significant role in the enhancement of photocatalytic activity. The results also revealed that the optimum molar ratio for the doping metal ions and TiO_2 is 1:99 and above this molar ratio, the structural and textural parameters of nano TiO_2 were affected. The entry of Mg^{2+} into the lattice of nano TiO_2 creates charge compensating anion vacancy, which may enhance the adsorption of 4-CP [17]. Further, the dopant ion Mg^{2+} with ionic radius (0.86 Å), larger than Ti^{4+} (0.75 Å) but smaller than O^{2-} (1.31 Å), can either isomorphously substituted or interstitially introduced into the matrix of nano TiO_2 to produce oxygen vacancies which accelerate the transition and nanocrystallite growth of anatase nano TiO_2 [32]. The formation of Ti–O–Mg inhibits the transition of TiO_2 phase and prevents the agglomeration of TiO_2 nano particles and growth of rutile phase. Hence, the entry of Mg^{2+} ions into the TiO_2 lattices suppressed the particle growth and consequently increased the band gap value of nano TiO_2, which minimized the electron–hole recombination during the photocatalytic degradation of organic compounds [33]. The framework substitution of Mg^{2+} in TiO_2 lattice is also confirmed from the FT-IR spectrum of acid washed catalyst. In addition, leaching of metal ions from the TiO_2 lattice during the photocatalytic degradation of 4-CP was also not observed. In the case of Ba^{2+} doped nano TiO_2, no evidence for the isomorphic substitution of Ba^{2+} was observed since the ionic radius of Ba^{2+} (1.49 Å) is higher than Ti^{4+}. The carbonate layer favoured the adsorption of 4-CP via hydrogen bonding interaction between phenolic OH groups and barium carbonate on nano TiO_2 surface.

Moreover, the enhancement in the photocatalytic degradation of 4-CP with Ba^{2+} doped nano TiO_2 can be envisaged as detailed below. Hydrogen peroxide formed as per Eq. (2) reacts with either barium carbonate or barium oxide to give barium peroxide as shown in Eqs. (3) and (4) respectively. Barium peroxide can minimize electron–hole recombination by capturing the conduction band electron in nano TiO_2 as shown in Eq. (5). Barium hydroxide like barium oxide or barium carbonate can also react with hydrogen peroxide to yield barium peroxide as shown in Eq. (6). In addition, barium hydroxide or barium oxide can react with 4-CP to give barium phenolate as per the Eqs. (7) and (8) by which the accumulation of 4-CP on the surface of nano TiO_2 can be enhanced. Such a dual role of Ba^{2+} doping in nano TiO_2 is suggested to be the cause for the enhanced activity. The reaction of hydrogen peroxide with barium carbonate is established by the release of CO_2 tested by physical mixing.

$$2e^- + O_2 + 2H^+ \rightarrow H_2O_2 \quad (2)$$

$$BaCO_3 + H_2O_2 \rightarrow BaO_2 + CO_2 + H_2O \quad (3)$$

$$BaO + H_2O_2 \rightarrow BaO_2 + H_2O \quad (4)$$

$$BaO_2 + 2e^- + 2H^+ \rightarrow Ba(OH)_2 \quad (5)$$

$$Ba(OH)_2 + H_2O_2 \rightarrow BaO_2 + 2H_2O \quad (6)$$

$$Ba(OH)_2 + 2CP \rightarrow Ba(CP)_2 + 2H_2O \quad (7)$$

$$BaO + 2CP \rightarrow Ba(CP)_2 + H_2O \quad (8)$$

In order to investigate the recyclable efficiency of the catalyst, the suspension (catalyst) after degradation of 4-CP was filtered, washed several times with distilled water and dried at 200 °C. The catalyst was used again for photocatalytic study. The TOC removal efficiency of the recycled catalyst decreased significantly and about 30% decrease in efficiency was observed after four cycles. This may be due to blocking of active sites in the nanosized TiO_2 particles.

4. Conclusions

This study concludes that addition of nitrate of magnesium or barium is observed to influence the crystallization of anatase phase of TiO_2 significantly excluding rutile phase. The entry of Mg^{2+} into the lattice of nano TiO_2 is evidenced by XRD and FT-IR studies. Ba^{2+} is not observed to take the lattice position of nano TiO_2 due to its large ionic radius. The presence of Ba^{2+} as $BaCO_3$ on the external surface of nano TiO_2 is proved by XRD and FT-IR analysis. The change in the polarity of medium due to addition of metal nitrate during the preparation of nano TiO_2 in the sol–gel process is suggested to be the cause for the formation of exclusive anatase phase. The photocatalytic degradation of 4-CP over nanosize TiO_2 and Mg^{2+} and Ba^{2+} doped nano TiO_2 reveals higher activity for doped TiO_2. The enhanced adsorption of 4-CP over the catalyst surface and decrease in particle size as a result of Mg^{2+} and Ba^{2+} loadings are suggested to be the cause for higher activity of the catalysts. This study therefore suggests that the introduction of metal nitrate in general and alkaline earth metal nitrate in particular can effectively control the selective crystallization of anatase phase of nano TiO_2. This doped nano TiO_2 exhibits enhanced photocatalytic activity in the degradation of 4-CP.

Acknowledgements

The authors gratefully acknowledge the financial support from the University Grants Commission (UGC), New Delhi, through Centre with Potential for Excellence in Environmental Science in our University. The authors like to place on record the financial supports from UGC under special assistance—DRS and the Department of Science and Technology (DST), New Delhi, under FIST programme for the sophisticated equipments facilities in the Department. One of the authors, N. Venkatachalam is thankful to the CSIR, New Delhi, India for the award of Senior Research Fellowship.

References

[1] L.H. Keith, J. Pure Appl. Chem. 70 (1998) 2319.
[2] J. Theurich, M. Lindner, D.W. Bahnemann, Langmuir 12 (1996) 6368.
[3] A.K. Jain, V.K. Gupta, S. Jain, Suhas, Environ. Sci. Technol. 38 (2004) 1195.
[4] D. Chen, A.K. Ray, Appl. Catal. B: Environ. 23 (1999) 143.
[5] K.B. Sherrard, P.J. Marriott, R.G. Amiet, M.J. McCormick Ray, C.K. Millington, Chemosphere 33 (1996) 1921.

[6] M.A. Fox, M.T. Dulay, Chem. Rev. 93 (1993) 341.
[7] S. Anandan, A. Vinu, N. Venkatachalam, B. Arabindoo, V. Murugesan, J. Mol. Catal. A: Chem. 256 (2006) 312.
[8] M.R. Hoffman, S.T. Martin, W. Choi, D.W. Bahnemann, Chem. Rev. 95 (1995) 69.
[9] J.C. Yu, J.G. Yu, W.K. Ho, Z.T. Jiang, L.Z. Zhang, Chem. Mater. 14 (2002) 3808.
[10] P.V. Kamat, J.P. Chauret, R.W. Fessenden, J. Phys. Chem. 90 (1986) 1389.
[11] S. Sakthivel, M.V. Shankar, M. Palanichamy, B. Arabindoo, V. Murugesan, J. Photochem. Photobiol. A: Chem. 148 (2002) 153.
[12] N. Serpone, D. Lawless, J. Disdier, J.M. Hermann, Langmuir 10 (1994) 643.
[13] M. Anpo, M. Takeuchi, J. Catal. 216 (2003) 505.
[14] A. Di Paola, G. Marci, L. Palmisano, M. Schiavello, K. Uosaki, S. Ikeda, B. Ohtani, J. Phys. Chem. B 106 (2002) 637.
[15] W. Choi, A. Termin, M.R. Hoffman, J. Phys. Chem. 98 (1994) 13669.
[16] W. Ho, J.C. Yu, J. Mol. Catal. A: Chem. 247 (2006) 268.
[17] K. Nagaveni, M.S. Hegde, G. Madras, Giridhar Madras. J. Phys. Chem. B 108 (2004) 20204.
[18] N. Serpone, D. Lawless, R. Khairlutdinov, E. Pelizzetti, J. Phys. Chem. 99 (1995) 16655.
[19] G. Cerrato, L. Marchese, C. Morterra, Appl. Surf. Sci. 70 (1993) 200.
[20] A.P. Rivera, K. Tanaka, T. Hisanaga, Appl. Catal. B: Environ. 3 (1993) 37.
[21] H. Luo, C. Wang, Y. Yan, Chem. Mater. 15 (2003) 3841.
[22] N. Venkatachalam, M. Palanichamy, B. Arabindoo, V. Murugesan, J. Mol. Catal. A: Chem. 266 (2006) 158.
[23] M. Hirano, C. Nakahara, K. Ota, M. Inagaki, J. Am. Ceram. Soc. 85 (2002) 1333.
[24] JCPDS Reference Code: 00-001-0506.
[25] J. Nair, P. Nair, F. Mizukami, Y. Oosawa, T. Okubo, Mater. Res. Bull. 34 (1999) 1275.
[26] J. Zhang, T. Ayusawa, M. Minagawa, K. Kinugawa, H. Yamashita, M. Matsuoka, M. Anpo, J. Mol. Catal. A: Chem. 198 (2001) 1.
[27] H. Zhang, M. Finnegan, J.F. Banfield, Nano Lett. 1 (2001) 5.
[28] S. Sakthivel, M.C. Hidalgo, D.W. Bahnemann, S.-U. Geissen, V. Murugesan, A. Vogelpohl, Appl. Catal. B. 63 (2005) 31.
[29] S. Sakthivel, M.V. Shankar, M. Palanichamy, B. Arabindoo, D.W. Bahnemann, V. Murugesan, Water Res. 38 (2004) 3001.
[30] M.V. Shankar, S. Anandan, N. Venkatachalam, B. Arabindoo, V. Murugesan, Chemosphere 63 (2006) 1014.
[31] B. Neppolian, H.C. Choi, S. Sakthivel, B. Arabindoo, V. Murugesan, J. Hazar. Mater. B 89 (2002) 303.
[32] N.I. Al-Salim, S.A. Bagshaw, A. Bittar, T. Kemmitt, M.A. James, A.M. Mills, M.J. Ryan, J. Mater. Chem. 10 (2000) 2358.
[33] M.S.P. Francisco, V.R. Mastelaro, Chem. Mater. 14 (2002) 2514.